Modeling the chemical shift of lanthanide $4f$ electron binding energies

Pieter Dorenbos

Luminescence Materials Research Group, Faculty of Applied Sciences, Delft University of Technology, Mekelweg 15, NL-2629 JB Delft, Netherlands

(Received 22 October 2011; revised manuscript received 25 February 2012; published 6 April 2012)

Lanthanides in compounds can adopt the tetravalent [Xe]$4f^{n-1}$ (like Ce^{4+}, Pr^{4+}, Tb^{4+}), the trivalent [Xe]$4f^n$ (all lanthanides), or the divalent [Xe]$4f^{n+1}$ configuration (like Eu^{2+}, Yb^{2+}, Sm^{2+}, Tm^{2+}). The $4f$-electron binding energy depends on the charge Q of the lanthanide ion and its chemical environment A. Experimental data on three environments (i.e., the bare lanthanide ions where A = vacuum, the pure lanthanide metals, and the lanthanides in aqueous solutions) are employed to determine the $4f$-electron binding energies in all divalent and trivalent lanthanides. The action of the chemical environment on the $4f$-electron binding energy will be represented by an effective ambient charge $Q_A = -Q$ at an effective distance from the lanthanide. This forms the basis of a model that relates the chemical shift of the $4f$-electron binding energy in the divalent lanthanide with that in the trivalent one. Eu will be used as the lanthanide of reference, and special attention is devoted to the $4f$-electron binding energy difference between Eu^{2+} and Eu^{3+}. When that difference is known, the model provides the $4f$-electron binding energies of all divalent and all trivalent lanthanide ions relative to the vacuum energy.

DOI: 10.1103/PhysRevB.85.165107 PACS number(s): 71.55.−i, 78.55.−m, 71.70.Ch

I. INTRODUCTION

Lanthanide atoms with electron configuration [Xe]$4f^{n+1}5d^0\,6s^2$ or [Xe]$4f^n5d^1\,6s^2$, lose both $6s$ electrons and the $5d$ electron in compounds, and occasionally also one $4f$ electron, to attain the divalent [Xe]$4f^{n+1}$, the trivalent [Xe]$4f^n$, or the tetravalent [Xe]$4f^{n-1}$ configuration.[1] As a matter of convenience, we will reserve the letter n to represent the number of electrons in the $4f$ shell of the trivalent lanthanide ion with atomic number Z. $n+1$ then pertains to the divalent lanthanide with the same atomic number and $n-1$ to the tetravalent one with the same atomic number.

The questions addressed in this work relate to the $4f$-electron binding energy. What is the minimum energy required to bring an electron from the $4f$ shell to the vacuum? How does that energy depend on the number of electrons in the $4f$ shell (i.e., the atomic number of the lanthanide ion)? How does it depend on the charge Q of the lanthanide? And most importantly, how does this all change with changing chemical environment around the lanthanide ion? The simplest environment is just empty space or a vacuum. We are then dealing with the free (gaseous) lanthanide ions. Lanthanide ions as impurities in inorganic compounds are in an environment formed by the anions and cations of the host. The nature of a small poorly polarizable fluoride anion is quite different from that of a strongly polarizable sulfide or iodide anion, and this affects the $4f$-electron binding energy. Organic molecules form the environment in organolanthanide chemistry,[2,3] water molecules in aqueous solutions,[4–6] and pure lanthanide metals can be treated as a lattice of lanthanide ions that are immersed in a sea of conduction band electrons formed by the itinerant $5d$ and $6s$ electrons.

Figure 1 shows the $4f$-electron binding energy in the divalent and trivalent lanthanide impurities in YPO_4 relative to the binding energy of electrons at the top of the valence band. Such a so-called host referred $4f$-electron binding energy ($4f$-HRBE) scheme can be constructed routinely for many different compounds using relatively few experimental data as input.[7–9] The double zigzag curves connect the lanthanide $4f$-HRBE as a function of the number of electrons in the $4f$ shell. The lower curve (in blue) pertains to the trivalent lanthanide ion and the upper curve (in red) to the divalent lanthanide ion. The binding is strong when the $4f^m$ shell is half ($m = 7$) or completely filled ($m = 14$) and relatively weak when there are one or eight electrons in the $4f$ shell. The shape of the double zigzag curves appears rather invariant with the type of compound which enormously facilitates construction of $4f$-HRBE schemes. The following question arises: Are the double zigzag curves truly invariant, and why or why not? The energy difference $U(6,A)$ between the binding energy in the $4f$ shell of Eu^{2+} with that in Eu^{3+} depends on the type of compound A. It is about 7.5 eV in fluoride compounds, for YPO_4 it is 7.0 eV, and for sulfide compounds it tends to decrease to values near 6.0 eV (Ref. 10). Now the following question arises: What determines the value for $U(6,A)$, and can it be predicted beforehand? Our final question relates to the binding energy of $4f$-electrons relative to the vacuum level, or the vacuum referred binding energy (VRBE).

In this work we will answer the questions raised above by introducing a model that is based on the chemical shift of the $4f$-electron binding energy in compounds. We will first collect and analyze what is known on $4f$-VRBE values of the divalent and trivalent gaseous lanthanide ions. Next, $4f$-VRBE values for the divalent and trivalent lanthanides in the pure lanthanide metals, and finally for the lanthanides dissolved in water (aqueous solutions) are derived. The results will show that the chemical environment shifts the $4f$-electron binding energy upward (toward less strong bonding), and that shift appears larger for trivalent lanthanides than for divalent ones. Next, a fairly simple model will be proposed that explains these chemical shifts, and that relates the energy difference $U(6,A)$ to the size of the chemical shift and therewith to the absolute binding energy of $4f$-shell electrons.

II. RESULTS

A. $4f$-VRBE of the free lanthanide ions

The information on the $4f$-VRBEs of the free (gaseous) divalent lanthanide ions were analyzed and collected by Sugar

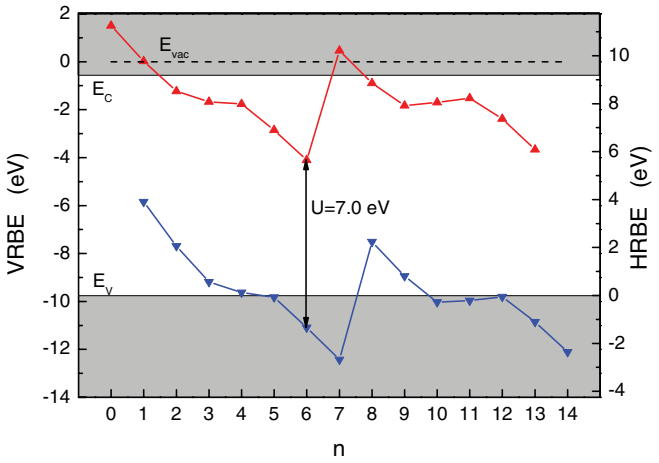

FIG. 1. (Color online) Host referred (right-hand energy scale) and vacuum referred (left-hand energy scale) $4f$-electron binding energy curves for the divalent (upper curve) and trivalent (lower curve) lanthanide ions in YPO_4. E_V and E_C are the binding energies at the top of the valence band and at the bottom of the conduction band.

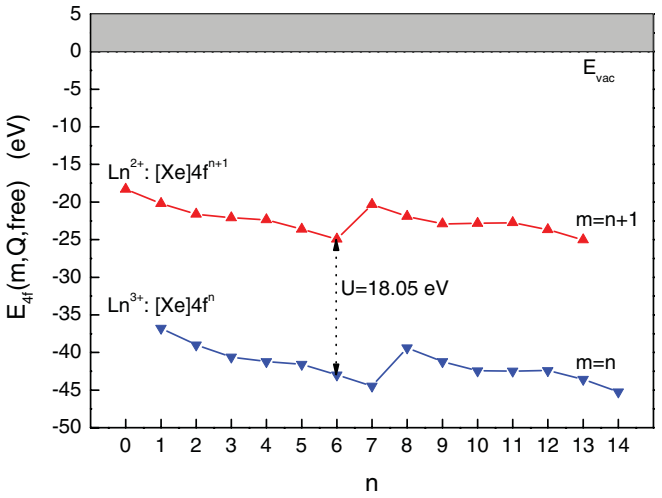

FIG. 2. (Color online) $4f$-VRBE curves for the free trivalent (lower curve) and free divalent (upper curve) lanthanide ions.

and Reader[11] in 1973. The values for all 14 lanthanide ions (La^{2+} with $n+1=1$ until Yb^{2+} with $n+1=14$) are compiled in column 3 of Table I. The $4f$-VRBE for divalent Nd, Pm, Sm, Eu, and Dy were estimated by Sugar and Reader by subtracting the (estimated) energy for the first $4f$-$5d$ transition and the (estimated) energy for the first $5d$-$6s$ transition from the experimentally known $6s$-VRBE. After the work by Sugar and Reader, Brewer[12] published new experimental values on the first $4f$-$5d$ transition in Nd^{2+} (1.892 eV), Sm^{2+} (3.038 eV), Eu^{2+} (4.198 eV), and Ho^{2+} (2.236 eV) and on the first $4f$-$6s$ transition in Eu^{2+} (5.715 eV). With these data the estimates by Sugar and Reader have been reevaluated. Employing the same method as used by Sugar and Reader, one obtains -24.92 eV for the $4f$-VRBE of Eu^{2+}. In the case of Nd^{2+}, Pm^{2+}, Sm^{2+}, and Dy^{2+} the energy of the first $5d$-$6s$ transition was reestimated to eventually arrive at the $4f$-VRBE values proposed in column 4 of Table I.

TABLE I. $4f$-VRBE of the free divalent and trivalent lanthanide ions from Sugar and Reader (Ref. 11), Johansson (Ref. 13), and the $4f$-VRBE proposed and used in this work. All energies are in eV.

n	Ln	$Q=2+$ Sugar	$Q=2+$ This work	$Q=3+$ Johansson	$Q=3+$ This work
0	La	−18.286	−18.286	–	–
1	Ce	−20.198	−20.198	−36.758	−36.758
2	Pr	−21.624	−21.624	−38.98	−38.98
3	Nd	−22.14	−22.102	−40.6	−40.6
4	Pm	−22.32	−22.369	−41.3	−41.2
5	Sm	−23.43	−23.601	−41.6	−41.6
6	Eu	−24.7	−24.92	−43.0	−42.97
7	Gd	−20.335	−20.335	−44.5	−44.5
8	Tb	−21.91	−21.91	−39.37	−39.37
9	Dy	−22.79	−22.89	−41.1	−41.2
10	Ho	−22.84	−22.84	−42.4	−42.4
11	Er	−22.74	−22.74	−42.4	−42.5
12	Tm	−23.68	−23.68	−42.5	−42.4
13	Yb	−25.03	−25.03	−43.56	−43.56
14	Lu			−45.25	−45.25

Column 5 of Table I compiles the $4f$-VRBE of the gaseous trivalent lanthanide ions from the work by Johansson.[13] That of Ce^{3+}, Pr^{3+}, Tb^{3+}, Yb^{3+}, and Lu^{3+} are accurate experimental data. The VRBEs compiled for the other lanthanides are estimates by Johansson with a claimed accuracy of ±0.2 eV. Thiel *et al.*[14] made similar estimates. The average values from Johansson and Thiel *et al.* are compiled in column 6 and will be regarded as the best available values for $E_{4f}(n,3+,\text{vacuum})$ with an estimated accuracy of ±0.1 eV.

In Fig. 2 the $4f$-VRBE curves $E_{4f}(n,3+,\text{vacuum})$ and $E_{4f}(n+1,2+,\text{vacuum})$ are shown against n. With such a presentation the $4f$-VRBE of Eu^{2+} with $n+1=7$ can be found vertically above that of Eu^{3+} with $n=6$. The energy difference

$$U(n,A) \equiv E_{4f}(n+1,2+,A) - E_{4f}(n,3+,A) \qquad (1)$$

is known as the $4f$-$4f$ Coulomb repulsion energy. It expresses the Coulomb repulsion experienced by an electron when it is added to the $4f$ shell of a lanthanide that already contains n electrons, and for the free Eu ion $U(6,\text{vacuum})$ amounts to 18.05 eV.

B. $4f$-VRBE in the lanthanide metals

To derive the $4f$-VRBE of the lanthanides in the pure lanthanide metals, we will combine four separate sets of experimental data: (1) data from bremsstrahlung isochromat spectroscopy (BIS), (2) data from x-ray photoelectron spectroscopy (XPS), (3) data on the work function Φ of the lanthanide metals, and (4) thermochemical data on the lanthanide metals.

Extensive and reliable XPS and BIS studies on all lanthanide metals were reported by Lang *et al.*.[15–17] The BIS data on the trivalent lanthanide metals provide the $4f$-HRBE of the divalent lanthanides relative to the Fermi energy $E_F(n) \equiv -\Phi(n)$ (i.e., relative to the binding energy of the electrons at the top of the conduction band). The BIS data

TABLE II. $4f$-HRBE in the lanthanide metals derived from BIS [$E_{\rm BIS}(n+1)$] and XPS [$E_{\rm XPS}(n)$] and the work function Φ. $E_{4f}(n+1,2+,A)$ and $E_{4f}(n,3+,A)$ are the $4f$-VRBE in the divalent and trivalent lanthanides in the lanthanide metals proposed and used in this work. The BIS value for Eu pertains to Eu^{+} and the XPS values for Eu and Yb pertain to Eu^{2+} and Yb^{2+}. The work function for Yb metal is an estimate. All energies are in eV.

n	Ln	$E_{\rm BIS}(n+1)$	$E_{\rm XPS}(n)$	Φ	$E_{4f}(n+1,2+,A)$	$E_{4f}(n,3+,A)$
0	La	5.31		2.96	1.97	–
1	Ce	3.46	-1.1 ± 0.8	2.97	0.351	−4.46
2	Pr	2.14	−3.33	2.96	−0.894	−6.41
3	Nd	1.72	−4.65	3	−1.22	−7.73
4	Pm	–	–	–	−1.40	−8.03
5	Sm	0.46	−5.07	2.85	−2.48	−8.20
6	Eu	*8.63*	*−1.5*	2.5	−3.72	−9.33
7	Gd	4.04	−7.44	3.17	0.953	−10.7
8	Tb	2.76	−2.23	3.15	−0.492	−5.37
9	Dy	1.81	−3.86	3.25	−1.42	−6.99
10	Ho	1.93	−4.89	3.22	−1.28	−8.03
11	Er	2.15	−4.7	3.25	−1.10	−7.88
12	Tm	1.1	−4.57	3.1	−1.95	−7.64
13	Yb		*−1.27*	*2.75*	−3.23	−8.60
14	Lu		−7.02	3.25		−10.1

from[17] are gathered in Table II as $E_{\rm BIS}(n+1) \equiv E_{4f}(n+1,2+,\text{metal}) - E_F(n)$. Eu is divalent in Eu-metal and then $E_{4f}(8,1+,\text{metal}) - E_F(6)$ is probed with BIS; in other words the $4f$-HRBE of monovalent Eu^{+} relative to $E_F(6)$ in divalent Eu metal. XPS data are compiled in column 4 as the energy $E_{\rm XPS}(n) \equiv E_{4f}(n,3+,\text{metal}) - E_F(n)$ which is the same as the $4f$-HRBE of the trivalent lanthanide relative to $E_F(n)$ in the trivalent lanthanide metal. In the case of the divalent Eu and Yb metals, the $4f$-HRBEs of Eu^{2+} and Yb^{2+} relative to $E_F(6)$ and $E_F(13)$ of the divalent metals are obtained with XPS, respectively. The XPS data for Ce metal are less reliable because the XPS signal from the $4f$-electrons has relatively low intensity and is contained in the energy interval of the occupied conduction band.[17]

To derive the $4f$-VRBEs in lanthanide metals from the $4f$-HRBEs, the work function $\Phi(n) \equiv -E_F(n)$ needs to be known. Durakiewicz *et al.*[18] calculated $\Phi(n)$ for all lanthanide metals and made a comparison with experimental data.[19] The values derived from those works are compiled in column 5 of Table II. Experimentally Φ increases and the Fermi energy decreases by about 0.3 eV when going from Ce^{3+} ($n=1$) to Lu^{3+} ($n=14$) which is due to the lanthanide contraction.[18] The work function is significantly smaller for Eu and Yb metal because those are divalent metals. Subtracting the work function Φ from the $4f$-HRBEs in columns 3 and 4, the $4f$-VRBEs $E_{4f}(n+1,2+,\text{metal})$ and $E_{4f}(n,3+,\text{metal})$ are obtained. The results are shown in Fig. 3. Although data for Pm^{2+}, Pm^{3+}, Eu^{3+}, and Yb^{3+} $4f$-VRBE are still missing we can, as in Figs. 2 and 1, recognize the familiar double zigzag patterns. Unfortunately XPS and BIS do not provide us with reliable data on the $4f$-VRBE of Eu and Yb metals and we have to use additional data or methods to obtain better accuracy.

One such method was followed by Johansson[13] using thermochemical data. Binding energy data similar to those in Fig. 3 are obtained but with a claimed better accuracy. One may also use the universal shape of the double zigzag curves in the $4f$-HRBE schemes as in Fig. 1. It is expected (see also Sec. II D) that a slightly tilted version of those curves should apply to the lanthanide metals. The dashed curves in Fig. 3 are the result of, in the authors opinion, a best compromise between the tilted versions of the universal curves and the XPS, BIS, and thermochemical data on the lanthanide metals. Note that the Eu^{2+} and Yb^{2+} $4f$-VRBE experimental data points fall significantly below the dashed curve. Those data are derived from XPS experiments on divalent Eu and Yb metal whereas all other divalent lanthanide $4f$-VRBE data are from BIS experiments on the trivalent lanthanide metals. With BIS therefore the $4f$-VRBE of a divalent lanthanide in a trivalent metal and with XPS the $4f$-VRBE of a divalent lanthanide in a divalent metal is obtained. The chemical environments

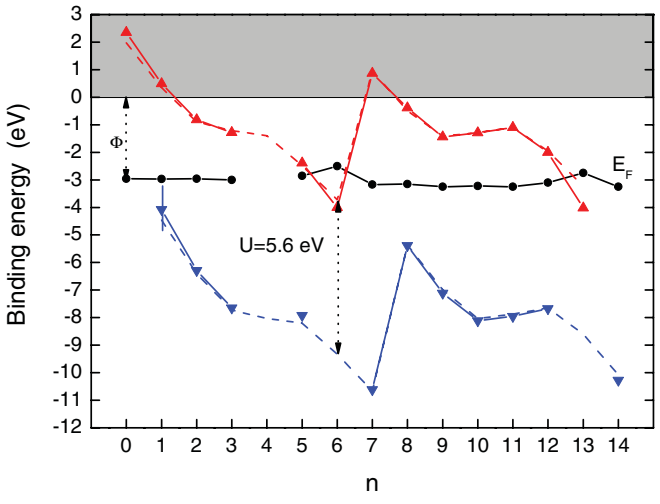

FIG. 3. (Color online) ▲ and ▼ data symbols connected with solid lines are the $4f$-VRBE for the divalent and the trivalent lanthanide ions in lanthanide metals, respectively, as derived from XPS and BIS. The two dashed curves connect the $4f$-VRBE values proposed in this work. •, the Fermi energy $E_F(n)$ in the lanthanide metals.

TABLE III. Standard Ln(II-III) and Ln(III-IV) oxidation potentials of lanthanides in aqueous solutions in volts and the derived absolute electrode potential in volts, which is equivalent to $4f$-VRBE in electron volts, for the divalent and trivalent lanthanides.

n	Ln	Ln(II-III)	Ln(III-IV)	$E_{4f}(n+1,2+,H_2O)$	$E_{4f}(n,3+,H_2O)$
0	La			1.61	
1	Ce		−1.74	0.13	−6.18
2	Pr		−3.2 ± 0.2	−1.13	−8.02
3	Nd		−5.0 ± 0.4	−1.57	−9.52
4	Pm			−1.66	−9.95
5	Sm	1.55		−2.75	−10.15
6	Eu	0.35		−4	−11.42
7	Gd			0.56	−12.75
8	Tb		−3.1 ± 0.2	−0.79	−7.84
9	Dy		−5.2 ± 0.4	−1.73	−9.27
10	Ho			−1.60	−10.36
11	Er			−1.42	−10.30
12	Tm	2.3 ± 0.2		−2.28	−10.13
13	Yb	1.15		−3.57	−11.18
14	Lu				−12.43

are thus not the same. The upper dashed curve is regarded to represent best the $4f$-VRBE of the *divalent* lanthanide ions in the *trivalent* lanthanide metals. The lower curve then represents best the $4f$-VRBE of the *trivalent* lanthanides in the *trivalent* lanthanide metals. The $4f$-VRBE values of these curves are compiled in columns 6 and 7 of Table II.

C. $4f$-VRBE of lanthanides in aqueous solutions

The redox potentials known in electrochemistry for several lanthanides in an aqueous solution are an additional source to derive $4f$-VRBE values. In this case the chemical environment is formed by water molecules. The Ce^{4+} to Ce^{3+} reduction potential in an aqueous solution has a well established value of 1.74 V relative to the standard hydrogen electrode.[20–22] The reduction potentials for Pr, Nd, Tb, and Dy are less well established and have been estimated by Nugent *et al.*.[20,21] Values are compiled as Ln(III-IV) oxidation potentials in column 4 of Table III. The Ln(II-III) oxidation potentials for Eu, Sm, and Yb are also well established, and the values together with an estimated value for Tm from Ref. 21 are compiled in column 3.

The oxidation potentials can be converted to $4f$-VRBE values by subtracting the absolute electrode potential of 4.44 V for the standard or normal hydrogen electrode.[23] The resulting data are shown in Fig. 4. As for the lanthanide metals and YPO_4 the double zigzag curves of $4f$-VRBE can be constructed through the data. The shape of the lower trivalent zigzag curve was taken similar to that of YPO_4, and it has been pinned by the well-established data point for Ce^{3+}. The $4f$-VRBE agrees very nicely with the ones derived from the predicted oxidation potentials in Ref. 21. Likewise the divalent zigzag curve is pinned to best reproduce the values for Eu^{2+}, Sm^{2+}, and Yb^{2+}. From the two $4f$-VRBE curves, a Coulomb repulsion energy of $U(6,H2O)$ of 7.4 eV is obtained, which is larger than that observed for YPO_4. Because the universal shape of the zigzag curves established from optical spectroscopy on lanthanide-doped inorganic compounds agree nicely with the data from oxidation potentials in electrochemistry, they can be utilized to estimate the oxidation potentials for all other lanthanides; one may simply add 4.44 V to the values in columns 5 and 6.

D. Chemical shift, Coulomb repulsion, and contraction tilt

Figure 5 collects the derived $4f$-VRBE data on the free lanthanide ions, aqueous solutions, and lanthanide metals. Defining the chemical shift for the $4f$-VRBE in Eu^Q ($Q = 2+$ or $3+$) in compound A as

$$E(Eu^Q,A) \equiv E_{4f}(Eu^Q,A) - E_{4f}(Eu^Q,\text{vacuum}) \qquad (2)$$

values of 31.55 and 33.64 eV are found for Eu^{3+} in water and in metal, respectively, as indicated by arrows 1 and 2 in Fig. 5. Figure 5 also shows that the chemical shifts for divalent Eu, see arrow 3, are smaller than for trivalent Eu, and consequently

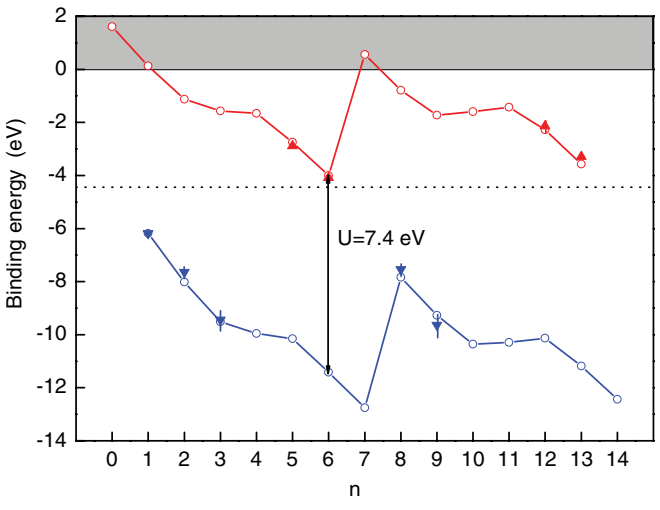

FIG. 4. (Color online) Solid triangular data symbols are $4f$-VRBE values as determined from reduction and oxidation potentials of lanthanides in aqueous solutions. The lower and upper zigzag curves connect the $4f$-electron binding energies of trivalent and divalent lanthanides in aqueous solutions. The dotted line at −4.44 eV represents the absolute electrode potential.

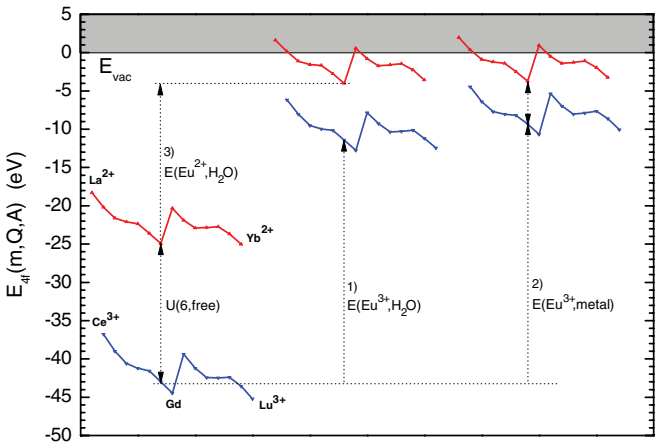

FIG. 5. (Color online) Scheme with the $4f$-VRBE $E_{4f}(m,Q,A)$ of the divalent ($Q = 2+$; upper curves) and trivalent ($Q = 3+$; lower curves) lanthanide ions. The curves on the left pertain to $A =$ vacuum, in the middle to $A = H_2O$, and on the right to $A =$ metal. The size of the chemical shift $E(Eu^Q, A)$ and the Coulomb repulsion energy $U(6,A)$ for Eu are indicated by the arrows.

$U(6,A)$ decreases from the free ion value 18.05 to 7.4 eV for water and to 5.61 eV for Eu metal. These results suggest that the energy difference $U(6,A)$ is somehow related to the size of the chemical shift. When such a relationship can be established, then knowledge on $U(6,A)$ alone will provide the chemical shift and therewith the absolute $4f$-electron binding energy.

The chemical environment also affects the shape of the double zigzag $4f$-VRBE curves. This is illustrated in Fig. 6 where the $4f$-VRBE curves for the trivalent lanthanides in vacuum, YPO_4, and metal are shown relative to $E_{4f}(6,3+,A)$. One observes that the double zigzag curve for the free lanthanides is being tilted due to the chemical environment,

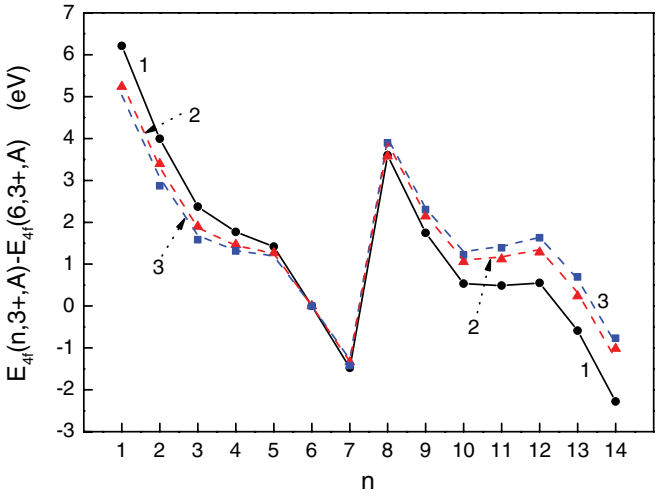

FIG. 6. (Color online) $4f$-electron binding energies relative to that in Eu^{3+}. • and solid curve 1 is for the free trivalent lanthanide ions, dashed curve 2 is obtained with a contraction tilt $\alpha(3+,A) = 0.11$ eV/pm on curve 1, dashed curve 3 is obtained with a contraction tilt $\alpha(3+,A) = 0.15$ eV/pm on curve 1. ■ data symbols pertain to the lanthanide metals. ▲ data symbols pertain to YPO_4.

and the size of the tilt for the lanthanide metals is slightly larger than for YPO_4. A similar observation was made by Pedrini *et al.*[24–26] when the $4f$-HRBE curve of divalent lanthanides in CaF_2, SrF_2, and BaF_2 as derived from photoconductivity studies was compared with the $4f$-VRBE curve for the free divalent lanthanides. It was explained by the lanthanide contraction that causes the surrounding anion ligands to move closer to the lanthanide impurity leading to a slightly larger chemical shift. An equation was proposed[24,26] that can be generalized to a more suitable form for this work as

$$E_{4f}(m,Q,A) = E_{4f}(m,Q,\text{vacuum}) + E(\text{Eu}^Q,A) + \alpha(Q,A)\Delta R(m), \quad (3)$$

where $\Delta R(m)$ is the difference in ionic radius of the lanthanide ion with m electrons in the $4f$-shell with that of the Eu ion. $\alpha(Q,A)$ will be called the *contraction tilt* parameter, and it defines the tilting of the double zigzag curve around the point at $E_{4f}(7,2+,A)$ when $Q = 2+$ (this is Eu^{2+}) and around $E_{4f}(6,3+,A)$ when $Q = 3+$ (this is Eu^{3+}). A variant of Eq. (3) was used by Thiel *et al.* to explain photoelectron spectroscopy (PES) data on various trivalent lanthanide-doped compounds and the pure lanthanide metals.[14,27,28]

III. DISCUSSION

The methods available to determine vacuum referred binding energies of electrons in the host energy bands or in impurities are very limited, and actually there are only photoelectron spectroscopy techniques like XPS and BIS. These techniques probe binding energies near the surface that require ultrahigh vacuum. The intention of this work is to determine the $4f$-VRBE of lanthanides in compounds with data from optical spectroscopy analyzed with a model on the chemical shift of $4f$-VRBE. To compare results from such modeling with the traditional techniques one should be very clear on what actually is being probed by either method. Figure 7(a) illustrates what happens when during a BIS experiment an electron is added (arrow 1) from the vacuum to the $4f$-shell of Eu^{3+} in hypothetical trivalent Eu metal. The Eu^{3+} ion with typical in-crystal ionic radius of 121 pm (Ref. 30) is at the center and surrounded by three electrons in the atomic cell of (estimated) radius 180 pm (Ref. 29). In the "complete screening picture" by Herbst *et al.*[31–33] the atomic cell always attains charge neutrality. That means that when an electron is added to a $4f$-shell (arrow 1) to convert Eu^{3+} into Eu^{2+} the less positive charge of Eu is instantly compensated by removal of a conduction band electron from the atomic cell (arrow 2). Note that sequential transfer of the two electrons is equivalent to the transfer of just one electron directly from the atomic cell to the $4f$ shell as indicated by arrow 3 in Fig. 7(a). With such a complete screening picture Herbst *et al.*[31–33] explained the large reduction of $U(n,A)$ from 18.05 eV to about 5.6 eV in the lanthanide metals. The typical "in crystal" ionic radius of Eu^{2+} (139 pm) is 18 pm larger than that of Eu^{3+} and the radius of the atomic cell of divalent Eu metal (204 pm) is about 24 pm larger than that of trivalent Eu metal.[29] This demonstrates that the transfer of an electron from the immediate environment to the $4f$-shell of Eu^{3+} causes an expansion of the Eu ion illustrated by the dashed circle in

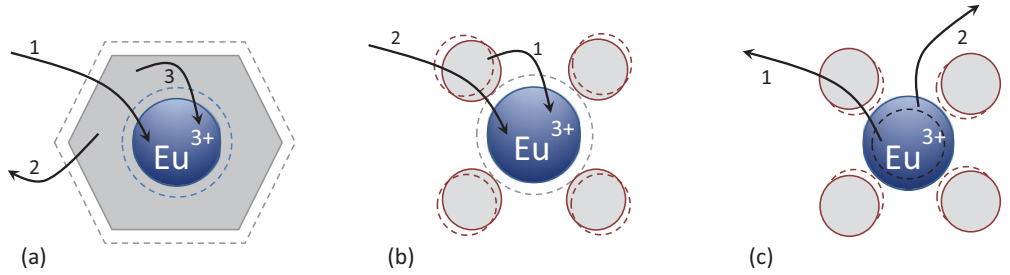

FIG. 7. (Color online) (a) Illustration of electron transfer during BIS on hypothetical trivalent Eu metal. (b) Illustration of electron transfer during BIS and during optical CT on Eu^{3+} as impurity in inorganic compounds. (c) Illustration of electron transfer during XPS and optical methods on Eu^{3+} as impurity in inorganic compounds.

Fig. 7(a) and an expansion of the atomic cell as illustrated by the dashed hexagon.

The $4f$-HRBE of Eu^{2+} as impurity in compounds is usually derived from the energy $E^{CT}(6,3+,A)$ needed for optically excited charge transfer or CT from a ligand to the $4f$-shell of Eu^{3+}.[7,34] Figure 7(b) illustrates what happens in an inorganic compound like YPO_4 where Eu^{3+} is surrounded by the ligands of its nearest oxygen anions. We will only deal with charge neutral compounds. This implies that the total charge Q_A of the chemical environment always balances against the charge Q of Eu (i.e., the ambient charge $Q_A = -Q$). After the electron transfer from a ligand to the $4f$ shell as indicated by arrow 1, the Eu ion expands and the ambient charge $Q_A = -3$ has instantly decreased to $Q_A = -2$. The less positive charge of Eu^{2+} will polarize or bind the surrounding oxygen ligands less strongly than Eu^{3+} did. As a result the anion ligands are instantly displaced outward as illustrated by the dashed circles. The massive nuclei remain stationary during the CT and may respond on the longer time scale of lattice vibrational frequencies ($\approx 10^{13}$ Hz). Collectively the change in the chemical environment due to the reduction in ambient negative charge, the polarization, the covalent bonding, and (on a longer time scale) the relaxation of the nuclei is known as *screening*.

With a BIS experiment on an inorganic compound like YPO_4:Eu the situation is different. Again an electron is added to the $4f$ shell as indicated by arrow 2 in Fig. 7(b) but this is not compensated by the removal of a bound electron from a nearest anion ligand. The $4f$-VRBE then refers to a binding energy in a $Q_A = -3$ chemical environment whereas $Q_A = -2$ with optical CT. This demonstrates that in presenting the $4f$-VRBE it is crucial to specify the state of the chemical environment immediately after the electron transfer has taken place. BIS probes *only for metallic compounds* the $4f$-VRBE in a $Q_A = -2$ chemical environment whereas optical CT *always* probes a $Q_A = -2$ chemical environment.

The $4f$-HRBE of the trivalent lanthanides in inorganic compounds obtained by optical methods is usually based on the total energy needed to excite an electron from the $4f$ shell to the conduction band where the electron is fully delocalized from the lanthanide. This implies that the electron is displaced far from the Ln^{4+} left behind. The electron transfer in the case of Eu^{3+} is illustrated by arrow 1 in Fig. 7(c). Due to the smaller ionic radius of Eu^{4+} and its higher positive charge, the surrounding anion ligands displace inward as indicated by the dashed circles. In the case of XPS an electron is excited from the $4f$ shell into the vacuum as indicated by arrow 2. In both XPS and the optical method the electron is removed far from the parent $4f$ shell and in both cases the ambient charge of the chemical environment after the removal is $Q_A = -3$. In that respect the XPS and optical method probe more alike chemical environments than in the case of BIS and optical CT. However, the optical method often involves as first step the excitation of a $4f$ electron to the $5d$ shell and as a second step a thermal ionization to the conduction band. This implies that the ionization process takes place on a longer time scale than with XPS enabling the nuclei to relax to lower energy lattice positions. Therefore also XPS and the optical methods do not probe the same binding energies.

A. The chemical shift model

Consider the Eu^Q ions with $[Xe]4f^6$ or $[Xe]4f^7$ electron configuration embedded in a chemical environment A with total ambient charge $Q_A = -Q$. The interaction between that chemical environment and the $4f$ electrons is highly complex involving exchange interactions, Coulomb interactions, polarization, correlation effects, covalency, and so on.[27] It requires a full quantum mechanical treatment, and even then computational methods are not at a level to routinely and accurately generate $4f$-VRBEs. This work intends to establish a model that with minimal experimental data and some plausible assumptions as input is able to generate chemical shift values and the $4f$-VRBEs of the lanthanides. The idea is the following. The chemical shift is simply represented by the Coulomb interaction between the $4f$ electron located near the nucleus and a total charge of $Q_A = -2$ for Eu^{2+} and $Q_A = -3$ for Eu^{3+} that is located at a distance $R_Q(A)$ from that nucleus. This distance will be called the *screening distance*, and together with Q_A they are the only two parameters that characterize the chemical environment. The chemical shift is given by

$$E(Eu^Q, A) = \frac{Q}{4\pi\epsilon_0}\frac{e^2}{R_Q(A)}, \tag{4}$$

where Q is in units of elementary charge.

From the free ion data in Table I and the lanthanide metal data in Table II it follows that the chemical shift $E(Eu^{2+}, \text{metal}) = 21.20$ eV and $E(Eu^{3+}, \text{metal}) = 33.64$ eV. Then from Eq. (4), $R_{3+}(\text{metal}) = 128.4$ pm and $R_{2+}(\text{metal}) = 135.8$ pm. These screening distances compare with the Shannon[30] in-crystal ionic radii of 121 pm for Eu^{3+} and 139 pm

for Eu^{2+} and the metallic atomic cell radii of (estimated) 180 and 204 pm (Ref. 29). The proposed chemical shift model therefore suggests that the ambient charge Q_A is, on average, located closely around the lanthanide ion and inside the atomic cell. Intuitively this is to be expected because such close contact leads to energy minimization. The model also shows that effectively the 2− ambient charge around Eu^{2+} in (hypothetical) trivalent Eu metal is 7.6 pm further from the nucleus than that around Eu^{3+} in (hypothetical) trivalent Eu metal. This all reflects quite satisfactorily the events outlined in Fig. 7(a).

In principle Eq. (4) will apply to every spherically symmetric charge distribution that does not extend beyond the screening distance R_Q. The $4f$ electron is not located at a fixed position close to the nucleus, but has a charge distribution density that is given by its $4f$ wave function. For example, the calculated $4f$ wave function for Ce^{3+} in BaF_2 is maximum near 22 pm (Ref. 35). Fortunately the part of the wave function extending beyond a screening distance of typically 140 pm is quite insignificant, and for such a distributed charge, Eq. (4) remains a good representation for chemical shift. Whether the ambient charge is concentrated as one point charge at distance R_Q, or distributed over several points is also irrelevant. Actually a nonsymmetrical ambient charge distribution will cause a crystal field splitting of the states of the $4f$ configuration. The size of such $4f$-level splitting is known to be very small, and the effect on the $4f$-VRBE can be ignored. One may equally well distribute the ambient charge over a shell of radius R_Q. In another context Fadley *et al.*[36] used such a classical charged shell approximation as a representation of chemical shift.

The $4f$-VRBE for divalent Eu can now be written as

$$E_{4f}(7,2+,A) = -24.92 + \frac{2 \times 1440}{R_{2+}(A)} \tag{5}$$

and for trivalent Eu

$$E_{4f}(6,3+,A) = -42.97 + \frac{3 \times 1440}{R_{3+}(A)}, \tag{6}$$

where energy is in electron volts and distance in picometers. Lines 1 and 2 in Fig. 8 show the above two $4f$-VRBE lines. For each environment the $4f$-VRBE of divalent Eu and trivalent Eu can be located somewhere on those binding energy lines by the appropriate choice of the effective screening distances. On the far left at $1/R_Q = 0$, the $4f$-VRBE of the free ion Eu^{2+} and Eu^{3+} are located. Eu atoms have electron configuration $[Xe]4f^7 6s^2$ that can be seen as a divalent $[Xe]4f^7$ Eu ion plus two electrons in its own $6s$ shell. The experimental $4f$-VRBE is −9.99 eV (Ref. 37), which corresponds with $R_{2+} = 193$ pm in Fig. 8. This screening distance compares with the 202 pm calculated for the maximum in the radial expectation value of the $6s$ orbital in Eu atoms by Mann.[38] Bringing one of the two $6s$ electrons to the $5d$ orbital with a maximum in the radial expectation value that is closer to the nucleus should then increase the chemical shift and decrease the $4f$-VRBE. Indeed the $4f$-VRBE for Eu atoms in the $[Xe]4f^7 5d6s$ configuration is about −7.55 eV (Ref. 33), corresponding to an effective screening distance of 166 pm. The $4f$-VRBE data for both atomic configurations are shown on line 1 in Fig. 8. Finally, the data for the $4f$-VRBE for Eu^{2+} and Eu^{3+} in (hypothetical) trivalent Eu metal and in aqueous solutions are shown on those two lines where the screening distance has further reduced.

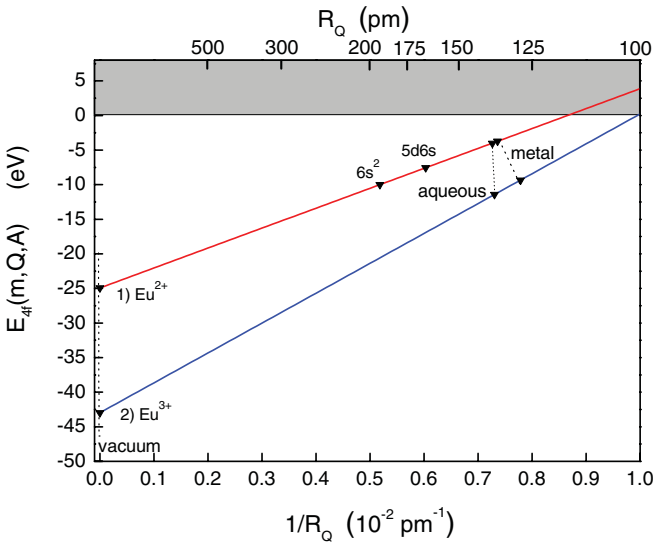

FIG. 8. (Color online) The $4f$-VRBE as function of the inverse screening distance for line 1 Eu^{2+} with $[Xe]4f^7$ configuration and line 2 Eu^{3+} with $[Xe]4f^6$ configuration. ▼ data symbols are experimentally derived binding energies.

Optical spectroscopy on lanthanide-doped compounds cannot provide direct information on where to place the $4f$-VRBE on the two lines in Fig. 8, but it does provide the value for $U(6,A)$. That knowledge is still not sufficient to uniquely locate the $4f$-VRBEs on the two binding energy lines. The problem can be solved if in addition a (plausible) relation between $R_{2+}(A)$ and $R_{3+}(A)$ can be established or assumed.

For (hypothetical) trivalent Eu metal it was found that R_{2+}(metal) is 7.43 pm larger than R_{3+}(metal). For Eu in an aqueous solution R_{2+} appears 0.74 pm larger than R_{3+}. From this scarce data we conclude that the screening distances for the divalent and trivalent lanthanides are not too different (<5 %), and since the divalent lanthanide is larger than the trivalent one, $R_{2+}(A)$ will be larger than $R_{3+}(A)$ for all chemical environments A. In metals, the electrons can freely adapt to the size difference between Eu^{2+} and Eu^{3+}. In compounds with strongly bonded anion ligands such adaptation is restricted. It is now tentatively assumed that the difference $R_{2+}(A) - R_{3+}(A)$ depends on the strength of binding of the electrons in the anion ligands. Therefore it will be relatively small for a fluoride compound like LaF_3 and largest for the lanthanide metals. The chemical shift also depends on the strength of binding, suggesting that $R_{2+}(A) - R_{3+}(A)$ scales with the size of the chemical shift or, equivalently, with $U(6,A)$. The following relation is proposed

$$\frac{R_{2+}(A)}{R_{3+}(A)} = \frac{R_{2+}(\text{metal})}{R_{3+}(\text{metal})} - \rho\left(\frac{U(6,A) - U(6,\text{metal})}{U(6,LaF_3) - U(6,\text{metal})}\right). \tag{7}$$

Here, LaF_3 with $U(6,LaF_3) = 7.51$ eV is chosen as a representative for a compound with strongly bonded anion ligands, and ρ is a constant that needs to be chosen for all chemical environments alike in a way to best reproduce experimental data on VRBEs. Figure 9 shows how for different values

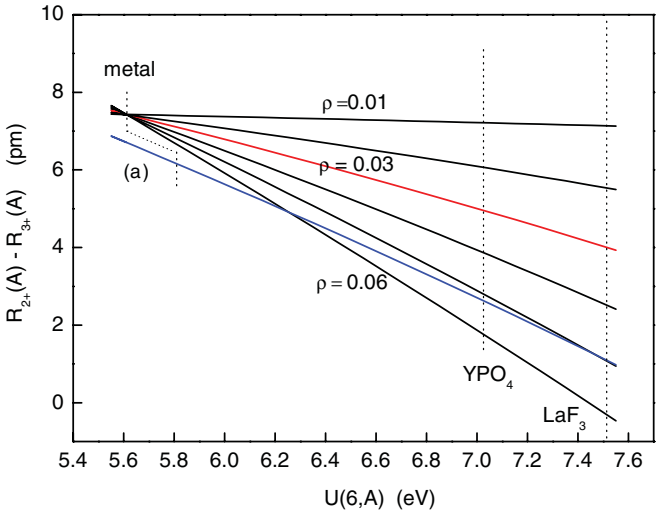

FIG. 9. (Color online) The difference between the R_{2+} and R_{3+} obtained with different values for ρ and with $U(6,\mathrm{LaF_3}) = 7.51$ eV and $R_{2+}(\mathrm{metal})/R_{3+}(\mathrm{metal}) = 1.0579$. Curve a is obtained with the proposed relation of Eq. (9).

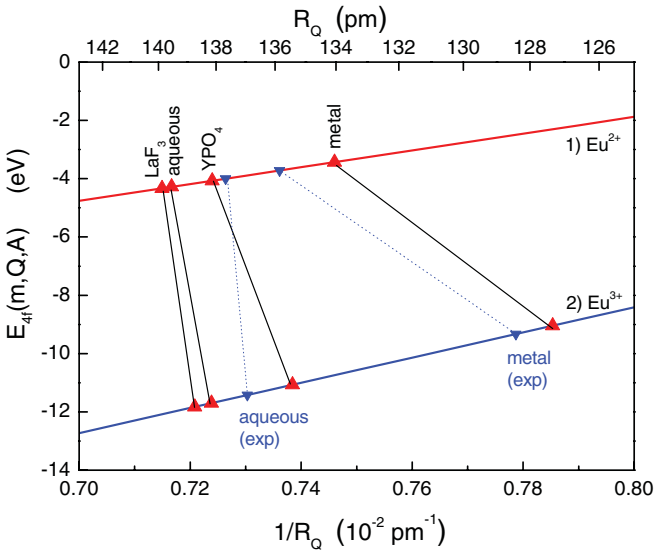

FIG. 10. (Color online) Lines 1 and 2 are the $4f$-VRBE lines for Eu^{2+} and Eu^{3+} as defined within the screening model. ▲, $4f$-VRBE data for Eu calculated by using Eq. (10) and $U(6,A)$ = 7.51, 7.42, 7.0, and 5.61 eV for LaF_3, aqueous solution, YPO_4, and Eu metal. ▼ are experimental $4f$-VRBE values for aqueous solutions and Eu metal.

for ρ, $R_{2+}(A) - R_{3+}(A)$ change with $U(6,A)$. For $\rho = 0.01$, $R_{2+}(A) - R_{3+}(A)$ is almost invariant with $U(6,A)$, and for $\rho = 0.06$, $R_{2+}(A) - R_{3+}(A)$ decreases almost linearly with $U(6,A)$ toward near zero for $A = \mathrm{LaF_3}$.

Equations (7), (1), (5), and (6) can be solved for the $4f$-VRBE energy in the divalent ions yielding

$$E_{4f}(7,2+,A) = -24.92 + \frac{18.05 - U(6,A)}{\frac{3R_{2+}(A)}{2R_{3+}(A)} - 1}. \qquad (8)$$

Knowledge of $U(6,A)$ together with an optimal value for ρ provides now sufficient information to uniquely determine the $4f$-VRBEs for divalent and trivalent Eu, and then with Eq. (3) for all the other lanthanide ions. In Eq. (7) the (hypothetical) trivalent Eu metal is used as a chemical environment of reference. One may equally well use Eu in aqueous solutions as the reference. However, one may question to what extend those two chemical environments are good representatives for lanthanide-doped compounds. A lanthanide metal is not a lanthanide-doped system but is 100% concentrated in one specific lanthanide, and in an aqueous solution the coordination number of water molecules around a lanthanide ion is not fixed. It is known to change from nine to eight when the size of the lanthanide increases.[4,5] Considering that also the values for the $4f$-VRBE of Eu in metals and aqueous solution contain an error that may be several 0.1 eV large it leaves us some room to adapt Eq. (7) to reach best consistency with the available data.

Curve a in Fig. 9 is obtained by using

$$\frac{R_{2+}(A)}{R_{3+}(A)} = 1.184 - 0.0235U(6,A) \qquad (9)$$

and then Eq. (8) becomes

$$E_{4f}(7,2+,A) = -24.92 + \frac{18.05 - U(6,A)}{0.777 - 0.0353U(6,A)}. \qquad (10)$$

At this stage the chosen values for the two constants in Eq. (9) may seem quite arbitrary, but it will turn out in forthcoming work that they do provide binding energy data that are consistent with available experimental data. For example, Pong and Inouye[39] reported a threshold for photoelectron emission from LaF_3 of 11.7 ± 0.3 eV, and also with photoelectron spectroscopy techniques Thiel[27] found the top of the valence band at -11.7 eV. Adding the Eu^{3+} charge transfer energy $E^{CT}(6,3+,\mathrm{LaF_3}) = 7.4$ eV known from optical spectroscopy,[40] one obtains a $4f$-VRBE for Eu^{2+} of -4.3 eV. With the above chosen constants indeed $E_{4f}(7,2+,\mathrm{LaF_3}) = -4.3$ eV is obtained. This is also seen in Fig. 10, which is an enlarged part of Fig. 8. It shows the $4f$-VRBE of Eu metal, Eu in YPO_4, Eu in an aqueous solution, and Eu in LaF_3 on the binding energy lines 1 and 2 as obtained with Eq. (10). The experimentally found binding energies for the metal and aqueous solutions are also shown.

The $4f$-VRBE for Eu^{2+} in YPO_4 is at -4.10 eV and this then pins the entire $4f$-HRBE scheme for YPO_4 relative to the vacuum level. The right-hand HRBE scale in Fig. 1 is then transferred in the left-hand VRBE scale, and the binding energy at the top of the valence band $E_V(YPO_4)$ becomes -9.75 eV. This demonstrates that the application of the proposed chemical shift model enables to derive the binding energy at the top of the valence band of compounds. The model also predicts that the $4f$-VRBE for Eu^{2+} shows surprisingly small variation among the different compounds. Throughout the entire family of inorganic compounds $U(6,A)$ is always between 7.6 and 6.0 eV, which implies that the $4f$-electron binding energy in Eu^{2+} is always to be found between -4.4 and -3.6 eV.

B. Relating the contraction tilt with chemical shift

The chemical shift model should be able to reproduce and explain the observed values for the contraction tilt $\alpha(Q,A)$

qualitatively and in part also quantitatively, see Fig. 6 and Eq. (3). Since Eq. (4) applies equally well to other lanthanides than Eu one may rewrite Eq. (3) as

$$E_{4f}(m,Q,A) = E_{4f}(m,Q,\text{vacuum}) + \frac{Q}{4\pi\epsilon_0}\frac{1}{R_Q(A) - f\Delta R(m)} \tag{11}$$

$$\approx E_{4f}(m,Q,\text{vacuum}) + E(Eu^Q,A)\left(1 + \frac{f\Delta R(m)}{R_Q(A)}\right). \tag{12}$$

Here it is assumed that the screening distance for a lanthanide other than Eu changes proportionally with the difference $\Delta R(m)$ between its ionic radius and that of Eu. f is the proportionality constant and $R_Q(A)$ pertains to the screening distances for Eu^Q. In the case of lanthanide-doped inorganic compounds, $f\Delta R(m)$ is caused by the lattice relaxation around the lanthanide impurity. From Eqs. (12) and (4) it follows that the contraction tilt increases quadratically with the chemical shift as

$$\alpha(Q,A) = f\frac{E(Eu^Q,A)^2}{1440Q}. \tag{13}$$

In lanthanide-doped inorganic compounds, lattice relaxation does not fully compensate for the ionic radius difference and f is typically 0.6–0.8.[26,41] With $f \approx 0.7$, Eq. (13) gives $\alpha(3+,\text{metal}) = 0.18\,\text{eV/pm}$ and $\alpha(2+,\text{metal}) = 0.10\,\text{eV/pm}$, which, considering the simple and even naive nature of the proposed chemical shift model, compare quite well with the experimental values of 0.11 and 0.075 eV/pm.

When $U(6,A)$ decreases from 7.6 eV in fluorides with tightly bonded anion ligands to around 6 eV in sulfides or selenides with weakly bonded ligands, one finds with Eqs. (13) and (8) that $\alpha(Q,A)$ increases by at most 20%. In that case the difference between the $4f$-VRBE of Eu^{2+} and Yb^{2+} changes by at most 0.13 eV. This is about the same size as the error margins in $4f$-VRBE values. The screening model therefore confirms that the double zigzag curves used to construct $4f$-HRBE schemes from optical spectroscopy data can be considered to good first approximation as invariant throughout the entire family of inorganic compounds.

IV. SUMMARY AND CONCLUSIONS

In this work the $4f$-VRBE in the divalent and trivalent lanthanide ions in three different chemical environments (i.e., in a vacuum, in aqueous solutions, and in the pure lanthanide metals) were determined and compared with each other. The results form the basis of a chemical shift model that relates the chemical shift of the $4f$-VRBE of the divalent lanthanide ions to that of the trivalent ones. The effect of the chemical environment on the binding energy has been represented by the Coulomb interaction of a total ambient charge $Q_A = -2$ or $Q_A = -3$ with the $4f$ electrons in the divalent or trivalent lanthanides, respectively. The type of chemical environment determines the effective distance of the ambient charge from the $4f$ electrons.

For the free lanthanide ions, the ambient charges are at infinite distance. Bringing both ambient charges from infinity closer to the lanthanide ions, the Coulomb interaction will raise the $4f$-electron energies as expressed with Eq. (4). If the two electrons are placed in the $6s$ shell around the Eu^{2+} ion we are dealing with Eu atoms. The effective screening distance is then 193 pm. Placing one electron in $5d$ and the other in $6s$ reduces the effective screening distance to 166 pm. The screening distance is further reduced for Eu^{2+} in compounds. In YPO_4 the lanthanides are surrounded by the charge carriers in the ligands and the nuclei, but the general picture remains the same. Effectively, the ambient charge Q_A is concentrated in the nearest neighbor anion ligands closely around Eu^Q. Within the family of inorganic compounds the screening distance depends on the type of compound, and it decreases when electrons are less strongly bonded in the anions until the shortest value of 135.8 pm is reached for Eu^{2+} in (hypothetical) trivalent Eu metal.

The chemical shift model confirms that the $4f$-VRBE binding energy zigzag curves for YPO_4 and lanthanide metal can be obtained by a chemical shift and contraction tilt operation on the free lanthanide $4f$-VRBE curves as seen in Fig. 5. In particular, the model shows that the errors made by assuming constant values for the contraction tilt parameters (i.e., assuming that the zigzag curves are invariant, are insignificant throughout the entire family of inorganic compounds). This is a finding of much practical importance. One only needs to pin the $4f$-VRBE (or $4f$-HRBE) of one lanthanide in a compound to obtain the $4f$-VRBE (or $4f$-HRBE) for all other divalent and trivalent lanthanides in that same compound.

This work proposes that the screening distance for Eu^{2+} in a compound is related with that of Eu^{3+} in that same compound according to Eq. (9). Since $U(6,A)$ can be determined routinely from optical spectroscopy on lanthanide-doped compounds, Eq. (10) provides a new tool to not only determine the $4f$-VRBE of divalent and trivalent lanthanides but also the binding energy E_V of the electrons at the top of the valence band in inorganic compounds.

[1] P. F. Lang and B. C. Smith, Journal of Chemical Education **87**, 875 (2010).
[2] W. J. Evans, Inorg. Chem. **46**, 3435 (2007).
[3] J. Thompson, V. Arima, Y. Zou, R. Fink, E. Umbach, R. Cingolani, and R. I. R. Blyth, Phys. Rev. B **70**, 153104 (2004).
[4] Y. Kaizu, K. Miyakawa, K. Okada, H. Kobayashi, M. Sumitani, and K. Yoshihara, J. Am. Chem. Soc. **107**, 2622 (1985).
[5] K. Okada, Y. Kaizu, H. Kobayashi, K. Tanaka, and F. Marumo, Mol. Phys. **54**, 1293 (1985).
[6] A. G. Svetashev and M. P. Tsvirko, Opt. Spectrosc. (USSR) **56**, 515 (1984).
[7] P. Dorenbos, A. H. Krumpel, E. van der Kolk, P. Boutinaud, M. Bettinelli, and E. Cavalli, Opt. Mater. **32**, 1681 (2010).

[8]P. Dorenbos, T. Shalapska, G. Stryganyuk, A. Gektin, and A. Voloshinovskii, J. Lumin. **131**, 633 (2011).
[9]P. Dorenbos, A. J. J. Bos, and N. R. J. Poolton, Phys. Rev. B **82**, 195127 (2010).
[10]A. Bessiere, P. Dorenbos, C. W. E. van Eijk, E. Yamagishi, C. Hidaka, and T. Takizawa, J. Electrochem. Soc. **151**, H254 (2004).
[11]J. Sugar and J. Reader, J. Chem. Phys. **59**, 2083 (1973).
[12]L. Brewer, *Systematics and the Properties of the Lanthanides*, edited by S. P. Sinha (D. Reidel, Dordrecht, The Netherlands, 1983), p. 17.
[13]B. Johansson, Phys. Rev. B **20**, 1315 (1979).
[14]C. W. Thiel, Y. Sun, and R. L. Cone, J. Mod. Opt. **49**, 2399 (2002).
[15]J. K. Lang, Y. Baer, and P. A. Cox, Phys. Rev. Lett. **42**, 74 (1979).
[16]Y. Baer and J. K. Lang, J. Appl. Phys. **50**, 7485 (1979).
[17]J. K. Lang, Y. Baer, and P. A. Cox, J. Phys. F **11**, 121 (1981).
[18]T. Durakiewicz, S. Halas, A. Arko, J. J. Joyce, and D. P. Moore, Phys. Rev. B **64**, 045101 (2001).
[19]H. B. Michaelson, J. Appl. Phys. **48**, 4729 (1977).
[20]L. J. Nugent, R. D. Baybarz, and J. L. Burnett, J. Inorg. Nucl. Chem. **33**, 2503 (1971).
[21]L. J. Nugent, R. D. Baybarz, J. L. Burnett, and J. L. Ryan, J. Phys. Chem. **77**, 1528 (1973).
[22]L. R. Morss, Chem. Rev. **76**, 826 (1976).
[23]S. Trasatti, Pure Appl. Chem. **58**, 955 (1986).
[24]C. Pedrini, D. S. McClure, and C. H. Anderson, J. Chem. Phys. **70**, 4959 (1979).
[25]D. S. McClure and C. Pedrini, J. Phys. Colloques **46**, C7-397 (1985).
[26]C. Pedrini, F. Rogemond, and D. S. McClure, J. Appl. Phys. **59**, 1196 (1986).
[27]C. W. Thiel, Ph.D. thesis, Montana State University, 2003.
[28]C. W. Thiel, H. Cruguel, H. Wu, Y. Sun, G. J. Lapeyre, R. L. Cone, R. W. Equall, and R. M. Macfarlane, Phys. Rev. B **64**, 085107 (2001).
[29]*Handbook of the physics and chemistry of rare earths*, Vol. 1, edited by Karl A. Gschneidner Jr. and Le Roy Euring, (North-Holland Publishing Company, Amsterdam, 1978), Table 2.13, p. 216.
[30]R. D. Shannon, Acta Crystallogr. Sect. A **32**, 751 (1976).
[31]J. F. Herbst, D. N. Lowy, and R. E. Watson, Phys. Rev. B **6**, 1913 (1972).
[32]J. F. Herbst, R. E. Watson, and J. W. Wilkins, Phys. Rev. B **13**, 1439 (1976).
[33]J. F. Herbst, R. E. Watson, and J. W. Wilkins, Phys. Rev. B **17**, 3089 (1978).
[34]P. Dorenbos, J. Phys.: Condens. Matter **15**, 8417 (2003).
[35]J. Andriessen, P. Dorenbos, and C. W. E. van Eijk, Phys. Rev. B **72**, 045129 (2005).
[36]C. S. Fadley, S. B. M. Hagstrom, M. P. Klein, and D. A. Shirley, J. Chem. Phys. **48**, 3779 (1968).
[37]S. T. Lee, S. Suzer, E. Matthias, R. A. Rosenberg, and D. A. Shirley, J. Chem. Phys. **66**, 2496 (1977).
[38]J. B. Mann and J. T. Waber, Atomic Data **5**, 201 (1973).
[39]W. Pong and C. S. Inouye, Opt. Soc. Am. **68**, 521 (1978).
[40]P. Dorenbos, J. Lumin. **111**, 89 (2005).
[41]P. Dorenbos, J. Phys.: Condens. Matter **15**, 2645 (2003).